ACS APPLIED MATERIALS & INTERFACES

Research Article

www.acsami.org

# Nanostructured Multifunctional Surface with Antireflective and Antimicrobial Characteristics

Sohee Kim,[†,§] Une Teak Jung,[†] Soo-Kyoung Kim,[‡] Joon-Hee Lee,[‡] Hak Soo Choi,[†,§] Chang-Seok Kim,[†] and Myung Yung Jeong*[,†,§]

[†]Department of Cogno-Mechatronics Engineering and [‡]Department of Pharmacy, College of Pharmacy, Pusan National University, Busan, 609-735, South Korea

[§]Division of Hematology/Oncology, Department of Medicine, Beth Israel Deaconess Medical Center and Harvard Medical School, Boston, Massachusetts 02215, United States

**ABSTRACT:** Functional polymeric films with antireflective and hydrophobic properties have been widely used for electronic device displays. However, the design of such functional films with an antimicrobial characteristic has been a challenge. We designed a nanostructured surface using a rigorous coupled-wave analysis to obtain a period of 300 nm and an aspect ratio of 3.0 on a flat poly(methyl methacrylate) film. The fabricated nanostructure was hydrophobic and exhibited the desired optical characteristics with a reflectance of less than 0.5% over the visible wavelength range. Furthermore, the nanoimprinted polymer film exhibited antimicrobial characteristics and low adhesion when compared with the corresponding flat surface. The results suggest that the nanostructured surface designed in this study is multifunctional and should be suitable for the production of protective optical and hygienic polymer films for the displays of portable electronic devices.

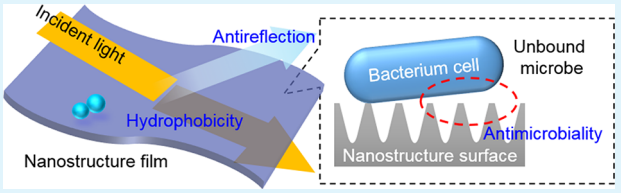


**KEYWORDS:** *nanopatterning, antireflective surface, antimicrobial surface, multifunctional film*

## INTRODUCTION

Recent advancements in information technology for portable devices demand functional optical films to protect displays while maximizing incident light. Significant efforts have focused on the development of antireflective surfaces using multilayer coatings and nanostructured patterning.[1] The degree of light reflection at a multilayer coated surface can be decreased by exploiting the phenomenon of destructive interference that occurs at the surfaces of the different layers.[1] However, the reflection typically appears only at a few specific wavelengths, such as within the range of 500−700 nm, and the variety of materials that can be deposited in multilayer coatings is limited.

Nanopatterning techniques have been developed based on natural structures, such as insect wings and eyes, the surfaces of which exhibit gradient refractive indices.[1−6] Such nature-mimicking nanostructured surfaces demonstrate greatly improved antireflective properties over a broad range of wavelengths.[1−3] Nanopatterning processes also improve the hydrophobic characteristics of flat-surface films, thus increasing antiwettability in addition to the clarity of the antireflective surface.[4−6]

Most recently, lotus-leaf-inspired nanostructures have been actively investigated because of their self-cleaning and antibiotic characteristics.[7−11] Indeed, such nanostructured surfaces have exhibited antibiofouling properties in that bacterial cells cannot attach to their surfaces. However, the antibiofouling properties of such nanostructured surfaces can be negatively affected if some portion of the nanopatterns is ruptured.[9,10]

In this study, we designed a nanostructured multifunctional surface on a conventional polymer film to achieve antireflective, antiwettable, and antibacterial functionalities. The key geometric factors considered for the nanostructured surface were roughness, period, height, and aspect ratio (height-to-radius ratio, h/r), which determined the final characteristics of the optical film. The effects of these design parameters on the nanopatterning were evaluated by measuring optical properties, wettability, and cell binding.

## MATERIALS AND METHODS

**Materials.** The chemical reagents and polymers used in the nanopatterning process were obtained from Dow Corning (Midland, MI) and Sigma-Aldrich (Saint Louis, MO), unless otherwise noted. Bottom antireflection coatings (BARC) and a thin photoresist (LX-429) were purchased from Dongjin Semichem, South Korea. Ormostamp resin was purchased from Micro Resist Technology (Berlin, Germany). Poly(methyl methacrylate) (PMMA) film (Goodfellow, USA) was used for nanostructure patterning, and an 8 in. silicon wafer was used as a master stamp substrate. An Optool DSX (Daikin Industries Ltd., Japan) treatment was used to apply an antisticking layer before the nanoimprinting process.

**Surface Design and Fabrication.** The nanostructure was designed using the rigorous coupled-wave analysis (RCWA) method,[12] which was employed to analyze the propagation of electromagnetic plane waves. Each unit cell of the simulated geometrical structure had

Received: September 12, 2014
Accepted: December 23, 2014
Published: January 5, 2015

  

DOI: 10.1021/am506254r
ACS Appl. Mater. Interfaces 2015, 7, 326−331

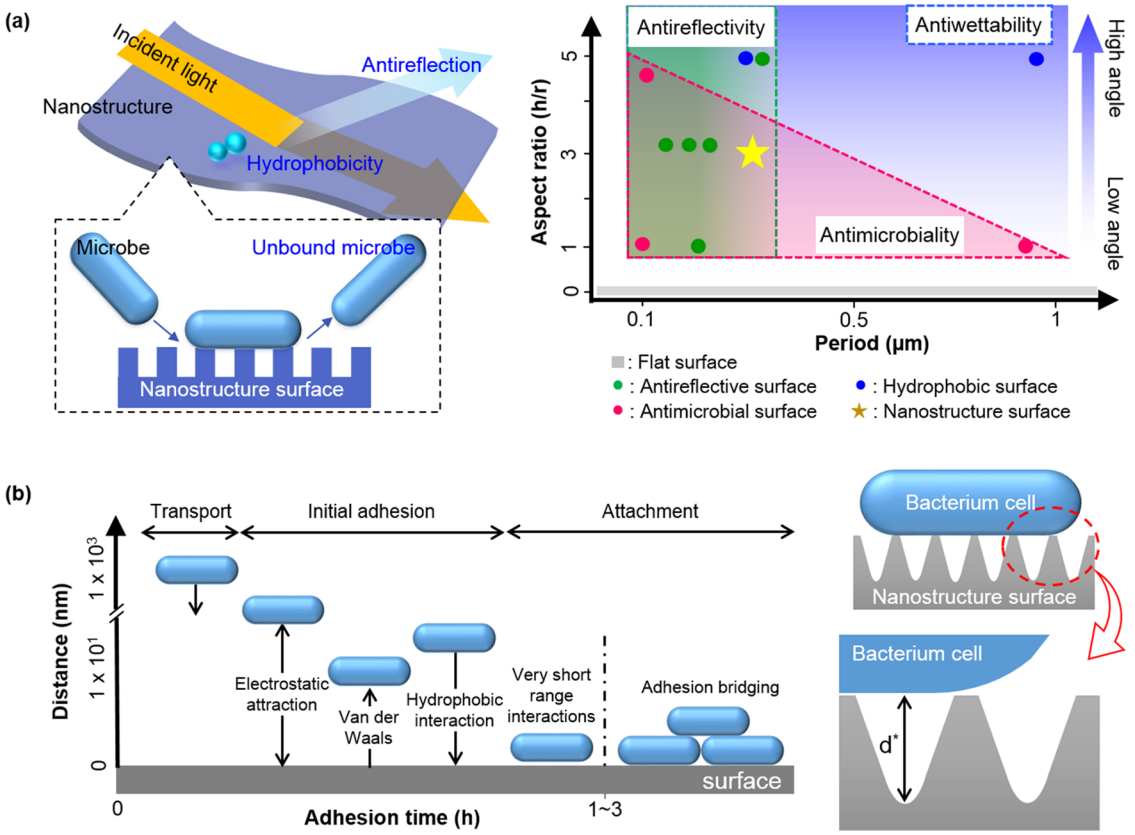


**Figure 1.** Design of nanostructured multifunctional surfaces: (a) conceptual illustration (left) and literature survey (right) for the design of multifunctional nanostructures with antireflectivity, antiwettability, and antimicrobial characteristics. The colored box delineates the optimal performance of each functionality reported in the literature,[1−11] and the yellow star indicates the ideal nanostructured surface used in this study. (b) Stages of bacterial attachment (left) depending on the distance between the cell and the surface[27] and a schematic view (right) of an antimicrobial nanostructured surface. *$d$ denotes the distance.

dimensions of 1 $\mu$m × 1 $\mu$m, and the cells formed a hexagonal, close-packed array. The patterning was applied using a 248 nm KrF excimer laser source (KrF Scanner System, ASML Co., Netherlands).[13] To form nanopillars on the polymer film surface, dry etching (LAM Research, Canada) was performed. Parabolic nanostructures were manufactured on the PMMA surface by depositing silicon dioxide ($SiO_2$) via a thermal oxidation process. In a subsequent process, the nanostructured surface was further modified via high-density plasma chemical vapor deposition using $SiO_2$ (Novellus Co., Canada), and thermal nanoimprint lithography was conducted on the PMMA film (Obducat, Sweden).[14] All stamps were coated with an antisticking layer (Optool DSX, Daikin Chemicals) for the subsequent demolding process.[15]

**Characterization of the Imprinted Surface.** The nanostructured surface was visualized using field emission scanning electron microscopy (FE-SEM S-4700, Hitachi High-Tech, Tokyo, Japan). The contact angle of the nanostructured surface was measured via the static sessile drop method using a Mouse-X system (SurfaceTech Co. Ltd., Seoul, South Korea), which was equipped with a charge-coupled device camera. Drops of deionized water were placed on at least three locations on the surface in an ambient environment, and the contact angles at these points were measured and averaged. The optical properties of the imprinted film were measured using a spectrometer (F20-EXR, Filmetrics, USA) for wavelengths in the range of 400−800 nm. The bottom surface of the imprinted film was blocked with a black tape to prevent interference between the top and bottom surfaces.

**Cell Culture and Cellular Binding Assay.** Two bacterial strains were grown in the following enriched media: lysogeny broth (LB) with 200 $\mu$g/mL carbenicillin (*Pseudomonas aeruginosa* PAO1) and LB with 50 $\mu$g/mL ampicillin (*Escherichia coli* DH5a). The bacterial cells were transfected with the green fluorescent protein (GFP)-expressing plasmid pAB1. After the bacteria had been inoculated in fresh LB medium for 24 h at 37 °C under gentle shaking (250 rpm), the bacteria were recovered and diluted in phosphate-buffered saline (PBS). The number of colony-forming units (CFU) per milliliter was confirmed through quantitative plate counts. To form a drip-flow-based biofilm, the bacteria were cultured overnight and diluted to OD600 = 0.1 in a fresh sample of LB. Then, 1 mL of this broth was placed on a slide. After 30 min of incubation, a 1% Bacto® tryptic soy broth (tryptone: 5.6 g/L, soytone: 1.6 g/L, NaCl: 1.6 g/L, dextrose: 0.8 g/L, and $K_2HPO_4$: 0.8 g/L) that contained 150 mg/mL carbenicillin and 1 mM isopropyl $\beta$-D-1-thiogalactopyranoside was continuously dropped onto the substrate at room temperature to form a biofilm at a flow rate of 0.2 mL/min. For a mammalian cell-binding test, the mouse myoblast cell line C2C12 was grown in a standard tissue culture dish (100 mm × 20 mm) in Dulbecco's minimum essential medium (DMEM), supplemented with 10% fetal bovine serum and 1% penicillin under 5% $CO_2$ and at 37 °C. When the cells attained 50 to 60% confluence, 10 $\mu$M ESNF13 dye[16] was added to the dish, and the cells were incubated for 20 min at 37 °C. The cells were trypsinized and seeded onto 12-well plates ($5 \times 10^4$ cells per well) and incubated daily. The cells were washed three times with culture medium prior to imaging. Cell adhesion was examined for a period of one week using a four-channel UV−vis−NIR fluorescence microscope.

**Fluorescence Microscopy and Data Analysis.** The fluorescence signals in the bacterial and mammalian cells were imaged using a Nikon TE 300 microscope system equipped with mercury and xenon excitation sources (Chiu Technical Corporation, Kings Park, NY) and an Orca-ER 12-bit camera (Hamamatsu, Bridgewater, NJ).[17,18] The GFP was measured using a 480/40 nm BP excitation filter and a 535/50 nm BP emission filter, whereas the NIR signal was imaged using a 650/45 nm BP excitation filter and a 700/35 nm BP emission filter


DOI: 10.1021/am506254r
ACS Appl. Mater. Interfaces 2015, 7, 326−331

(Chroma Technology, Brattleboro, VT). The obtained fluorescence images were calculated using ImageJ software, version 1.48v. A statistical analysis was conducted using a paired sample $t$ test: $*P < 0.05$, $**P < 0.01$, and $***P < 0.001$. The results were presented in the form of mean ± S.D., and curve fitting was performed using Origin software, version 8.1 (OriginLab Co., Northampton, MA).

## RESULTS

**Nanostructure Surface Design.** The key aspect of the design of this nanostructured surface for display films pertains to its multifunctional properties, such as antireflectivity, antiwettability, and antimicrobial behavior.[1−11] As shown in Figure 1a, conventional imprinted display films are hydrophobic, and their reflection is minimal. It is desirable for a functional nanostructured surface to also exhibit antiadhesion and antimicrobial characteristics. However, antimicrobial characteristics cannot be obtained in a larger period and aspect ratios because of the small size of bacterial cells; bacteria can adhere between pillars with a period greater than 1 $\mu$m. As shown in Figure 1b, bacterial cell attachment occurs in three consecutive steps: (1) transport to the film surface, (2) initial adhesion and attachment to the surface, and (3) short-range interactions and bridge formation. During the first two steps, physical contact causes the bacteria to approach the surface, and long-range interactions—including electrostatic interactions, van der Waals interactions, and hydrophobic interactions—dominate the initial adhesion of the bacteria. In the final step, chemical interactions between the bacteria and the polymer surface control the bacterial adhesion. Armed with this information, we designed a functional nanostructured surface with a period in the range from 200 to 400 nm and an aspect ratio between 1 and 3.

**Nanostructure Fabrication Process.** We designed a nanoimprinted polymeric film to fulfill all specified requirements based on the aspect-ratio/period chart presented in Figure 1a. The details of the nanopatterning process are depicted in Figure 2. First, to fabricate a large-area nanostructured surface, KrF laser lithography was applied to an 8 in. Si wafer.[13] A reticle was designed with a resolution of 300 nm, which was the optimal period size for the designed nanostructure. The nanostructured surface, which consisted of hexagonal lattices with a period of 300 nm, was then coated with the BARC photoresist to be 58 nm in thickness to reduce reflections and sidewall roughness. Subsequently, the nanostructured surface was coated with a 400 nm thick pattering photoresist (LX-429) on the 8 in. Si wafer. To ensure high antireflection performance, a 50 nm gap was maintained between the nanopillars through oxidation under optimized conditions at 1000 °C,[19] followed by dry etching with a combination of $Cl_2$ and HBr gases. Additionally, the shape was made parabolic to reduce the gap to less than 50 nm to ensure high performance. The thermal nanoimprinting process was performed at 135 °C under a pressure of 30 bar.

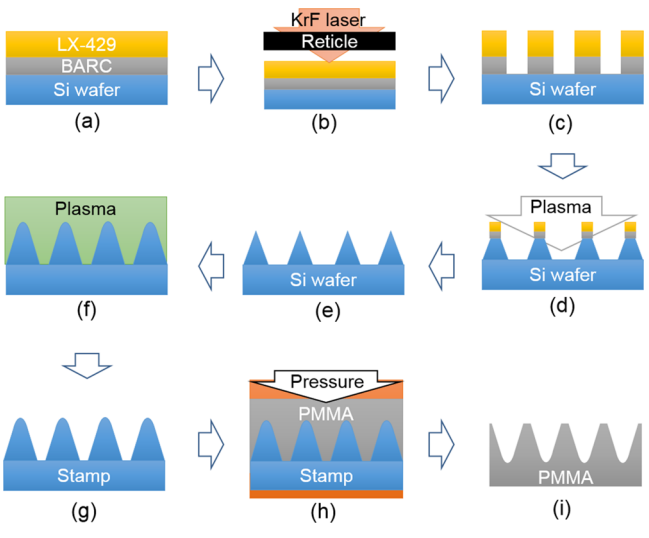


**Figure 2.** Fabrication process for the nanostructured surface: (a) photoresist coating, (b) exposure with a KrF laser, (c) developing of the photoresist, (d) plasma etching, (e) rinsing with $N_2$ gas, (f) chemical vapor deposition with high-density plasma, (g) rinsing with $N_2$ gas, (h) direct thermal imprinting, and (i) demolding of the imprinted film.

**Antiwettability and Antireflectivity of Nanostructure Surface.** After the completion of thermal nanoimprinting, the nanostructure imprinted on the PMMA film was characterized via SEM (Figure 3). The silicon stamp was well-structured with a resolution of 300 nm and a height of 490 nm, and top-view and cross-sectional (inserted) images are presented in Figure 3a. The nanoimprinted PMMA film was found to have a well-controlled pattern with a period of 300 nm and an aspect ratio of 3.0, as confirmed via SEM.

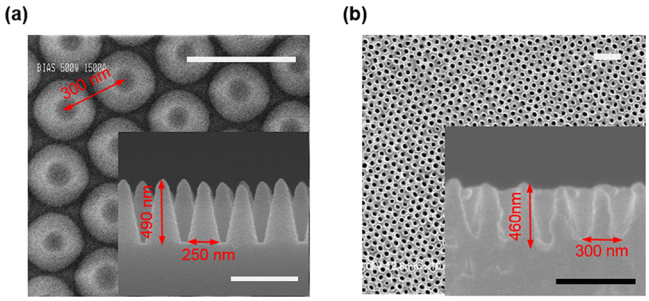


**Figure 3.** SEM images of the nanostructured surface: (a) a top view and cross-sectional view (inset) of the silicon master surface and (b) the nanostructured pattern on the PMMA film and a magnified cross-sectional image thereof (inset). Scale bars = 500 nm.

The wettability of the nanostructured PMMA film was determined by measuring the water contact angle (Figure 4a). The nanostructured surface was measured to be hydrophobic, exhibiting a contact angle of 114.5 ± 2°, whereas the bare PMMA film without nanostructure exhibited a contact angle of 67 ± 2°. The water contact angle increased gradually with increasing aspect ratio (data not shown).[5,20] The antireflection performance of the nanostructured surface was calculated using the RCWA method under conditions corresponding to a normal incident light,[12] in which the spectral region between 400 and 800 nm (visible wavelength range) was investigated in intervals of 10 nm. The nanostructure created on the film surface was found to be well oriented with a minimal reflectance of less than 0.5% (red line), which is coincident with the simulated result (blue dashed line). The minimum reflectance of the nanostructured surface was 0.37% at 550 nm, whereas the flat PMMA film surface (gray line) exhibited a reflectance of greater than 3% over the entire range of measured wavelengths.

**Antiadhesion and Antimicrobial Characteristics.** The nanoimprinted PMMA film was incubated with bacteria and mammalian cells to observe its antiadhesion and antimicrobial


DOI: 10.1021/am506254r
ACS Appl. Mater. Interfaces 2015, 7, 326−331

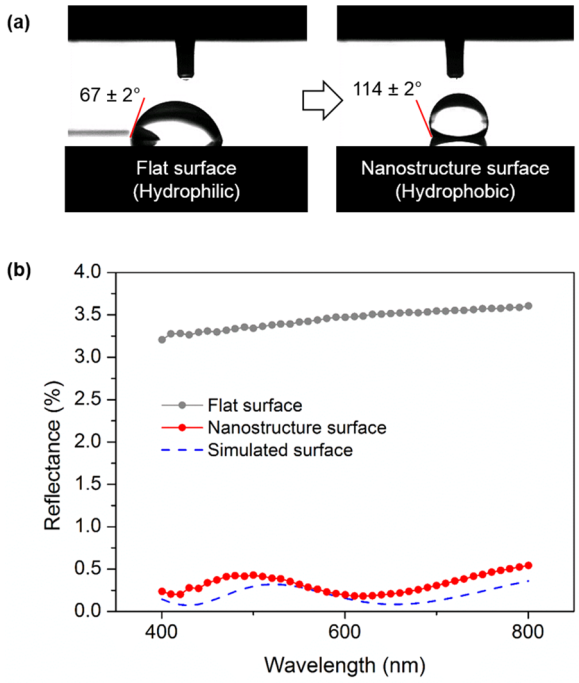


**Figure 4.** Hydrophobicity and antireflective characteristics of the nanostructured surface: (a) Contact angle measurements revealing the change in wettability of the PMMA films before and after nanoimprinting. (b) Reflectance profiles of the nanostructured surface (red line) and the flat PMMA surface (gray line) in the wavelength range between 400 and 800 nm. The simulated data (blue dashed line) for the nanostructured surface were calculated using the RCWA.

characteristics over a week of incubation time. As shown in Figure 5, the initial attachment (4 h of incubation) of *E. coli* on the nanostructured surface was significantly lower than that on the flat PMMA surface, whereas there was little to no difference in the initial attachment (1−4 h of incubation) of the *P. aeruginosa* and myoblast cells between the nanostructured and flat surfaces. However, the bacterial cell attachment on the flat surface increased significantly during incubation, and a significant difference ($^{**}P < 0.01$) between the nanostructured and flat surfaces was observed for both cell lines after 8 h of incubation. We also confirmed this result by incubating both films with C2C12 myoblast cells. The initial adhesion of the cells was similar on both film surfaces at 1 and 2 d ($P > 0.05$); however, the number of cells adhered on the nanostructured surface decreased significantly at 4 d ($^{***}P < 0.001$) because the hydrophobic nanostructured surface interfered with the cell−substratum interface during the proliferation and differentiation processes. It is well-known that such physical cell environments are important for cell survival, proliferation, differentiation and migration, for which the formation of adhesion to the cell substrate through an extracellular matrix protein is required.[21] Furthermore, most cells attached to the nanostructured surface died at 7 d because of the inhibition of growth and adhesion (Figure 5a).

Fluorescence imaging revealed differences in cell binding and proliferation on the nanostructured surface compared with the flat PMMA film. As shown in Figure 5b, the GFP signals of the bacterial cells on the flat surface were noticeably higher than those on the nanostructured surface throughout the incubation period. After 8 h of incubation, very few bacteria were observed on the nanostructured surface, reflecting the antibacterial property of the film resulting from the nanopatterning. NIR fluorescence imaging of the myoblast cells revealed clear differences in cell proliferation. The C2C12 cells were healthy and live on the flat PMMA film, whereas the imprinted nanostructure resulted in the formation of a restricted cell network and, eventually, cell death (7 d).

## DISCUSSION

Antireflective nanostructures have been inspired by objects in nature, such as insect wings and the surfaces of insect eyes. However, direct contact through the ears, nose, mouth, and hands can increase the degree of bacterial contamination and transference of microbes. To mitigate these risks, we manufactured an antireflective nanostructured surface to exhibit antimicrobial and antiadhesion properties. Initial adhesion and subsequent surface growth of bacterial cells on nonpolar hydrophobic surfaces are promoted because of favorable thermodynamics and physicochemical interactions such as van der Waals forces, electrostatic interactions, and hydrophobic interactions between the surface and cell membrane (Figure 1b).[22−24] In this study, however, we introduced an optimized roughness (i.e., roughness) on the hydrophobic PMMA surface and could avoid bacteria and mammalian cell growth remarkably on the nanostructured film. First, the 300 nm period of the fabricated nanostructure yielded a nanostructure with a 125 nm radius, which resulted in significantly improved antireflectivity. The parabolic shape of the nanostructure also improved the antireflective property of the nanostructured surface. The contact angle of the nanostructured surface can be described using the Wenzel model,[20,25]

$$\cos\theta_n = r\cos\theta_f \quad (1)$$

where $\theta_n$ is the contact angle of the nanostructured surface, $r$ is the roughness of the surface, and $\theta_f$ is the surface contact angle. This equation can be rewritten using the energy equilibrium theory, as follows:

$$r\gamma_{SV} = r\gamma_{SL} + \gamma_{LV}\cos\theta_n \quad (2)$$

where $\gamma_{SV}$, $\gamma_{SL}$, and $\gamma_{LV}$ are the surface tensions of the substrate−vapor, substrate−liquid, and liquid−vapor interfaces, respectively. On the basis of this equation, the roughness of our nanoimprinted surface could increase the measured contact angle ($\theta$) larger than 90°. Some superhydrophobic ($\theta > 150°$) and self-cleaning surfaces found in nature such as lotus leaves have potential antibiofouling characteristics because of multiple nanoscaled surface patterns.[5,20] However, unfortunately, our designed nanostructure showed little to no antibiofouling effect (data not shown). In this study, however, we found that the increase in the hydrophobic characteristics of the film induced by the fabrication of the nanostructure might have led to the manifestation of antiadhesion and antimicrobial properties. These indicate that the nanostructured polymer film is capable of preventing bacterial cell attachment to the surface. The worst-case scenario for the environmental conditions was assumed, in that the experiment was conducted in a liquid state. The results of this study indicate higher antiadhesion and antimicrobial performance in the air state compared with the liquid state. The bacterial cell adhesion force[26] combined with the Wenzel model can be expressed as follows:

$$\Delta F_{adh} = r\gamma_{BS} - r\gamma_{SL} - \gamma_{BL}\cos\theta_n \quad (3)$$


DOI: 10.1021/am506254r
ACS Appl. Mater. Interfaces 2015, 7, 326−331

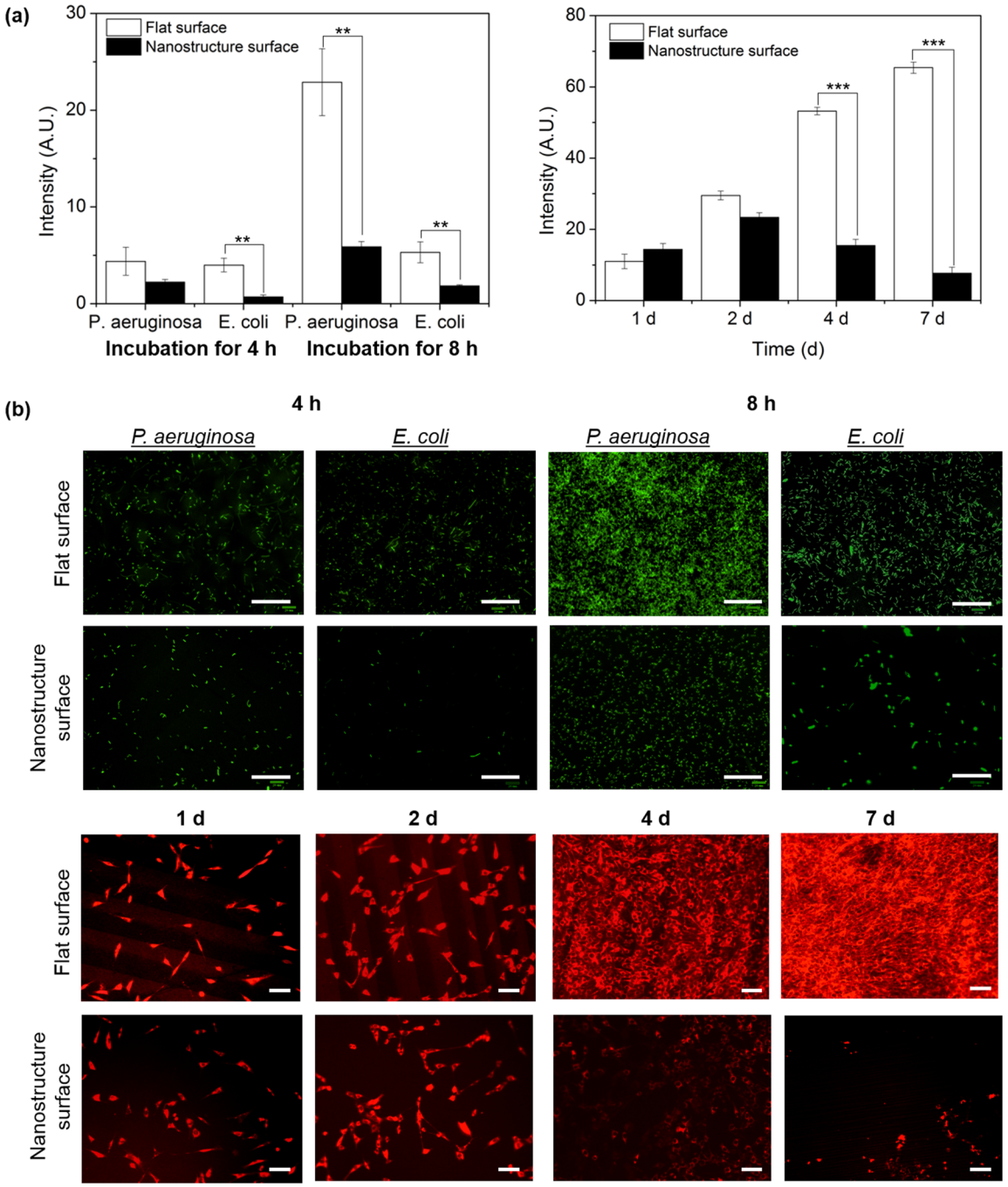


**Figure 5.** Bacterial and mammalian cell attachment to the flat and nanostructured surfaces: (a) Bacterial cells (left) and myoblasts (right) were incubated with each sample over time. ** $P < 0.01$; *** $P < 0.001$. (b) Fluorescence microscopic images of the bacterial cells (top) and the mammalian cells (bottom) on the flat and nanostructured surfaces. Pseudocolors of lime green and red are used for the GFP and 700 nm NIR channels, respectively, in these images. The NIR fluorescence images for each condition were acquired with identical exposure times and normalizations. Scale bars = 50 $\mu$m.

$$\cos\theta_n = r(\gamma_{BS} - \gamma_{SL})/\gamma_{BL} \quad (4)$$

where $\Delta F_{adh}$ is the change in the free energy of adhesion and $\gamma_{BS}$, $\gamma_{SL}$, and $\gamma_{BL}$ are the bacterium−surface, surface−liquid, and bacterium−liquid interfacial tensions, respectively. Equation 4 can be rewritten by assuming that $\Delta F_{adh} = 0$ when the cells adhere to the surface (Figure 1b). In this equation, the contact angle and the roughness $r$ are variables, whereas $\gamma_{BS}$, $\gamma_{SL}$, and $\gamma_{BL}$ are constants. The roughness $r$ is strongly related to the chart of aspect ratio and period presented in Figure 1a. Furthermore, the nanostructure can interrupt the physical contact of initial bacterial cell attachment via brushing effect, where the height of the nanopattern, $d$, exceeds the range of physical contact for cellular binding (Figure 1b). The fabricated nanostructures had a period of 300 nm and a height of 490 nm, both of which factors were important in achieving the observed antiadhesion and antimicrobial properties.

## CONCLUSION

In this study, we designed a nanostructured polymeric surface with improved antireflective and antimicrobial characteristics.


DOI: 10.1021/am506254r
ACS Appl. Mater. Interfaces 2015, 7, 326−331

First, the nanostructured polymer film exhibited a reflectance of less than 0.5% over a wide range of visible wavelengths. Second, the polymeric film surface was designed to be hydrophobic by means of simulated period and aspect ratio. A higher ratio and a shorter period increased the contact angle, thus causing the surface to be more hydrophobic. Most importantly, the proposed nanostructure inhibited the attachment of both bacterial and mammalian cells to the surface of the film. The fabricated nanostructure exhibited multifunctional characteristics indicating that it could be useful for the production of protective display films for portable electronic devices.

## AUTHOR INFORMATION

### Corresponding Author

*Phone: +82 51-510-3100. Fax: +82 51-510-1980. E-mail: myjeong@pusan.ac.kr.

### Notes

The authors declare no competing financial interest.

## ACKNOWLEDGMENTS

We thank D. J. Burrington, Jr. for editing and H. S. Jang for administrative assistance. This work was supported by grants from the Financial Supporting Project of Long-term Overseas Dispatch of PNU's Tenure-track Faculty, 2012.

## REFERENCES

(1) Chattopadhyay, S.; Huang, Y. F.; Jen, Y. J.; Ganguly, A.; Chen, K. H.; Chen, L. C. Anti-reflecting and Photonic Nanostructures. *Mater. Sci. Eng. R.* **2010**, *69*, 1−35.

(2) Yamada, N.; Kim, O. N.; Tokimitsu, T.; Nakai, Y.; Masuda, H. Optimization of Anti-reflection Moth-eye Structures for Use in Crystalline Silicon Solar Cells. *Prog. Photovoltaics* **2011**, *19*, 134−140.

(3) Park, H.; Shin, D.; Kang, G.; Baek, S.; Kim, K.; Padilla, W. J. Broadband Optical Antireflection Enhancement by Integrating Antireflective Nanoislands with Silicon Nanoconical-Frustum Arrays. *Adv. Mater.* **2011**, *23*, 5796−5800.

(4) Shin, J.-H.; Han, K.-S.; Lee, H. Anti-reflection and Hydrophobic Characteristics of M-PDMS Based Moth-eye Nano-patterns on Protection Glass of Photovoltaic Systems. *Prog. Photovoltaics* **2011**, *19*, 339−344.

(5) Park, K. C.; Choi, H. J.; Chang, C. H.; Cohen, R. E.; McKinley, G. H.; Barbastathis, G. Nanotextured Silica Surfaces with Robust Superhydrophobicity and Omnidirectional Broadband Supertransmissivity. *ACS Nano* **2012**, *6*, 3789−3799.

(6) Zhang, D.; Yu, W.; Hao, D.; Li, L.; Liu, H.; Lu, Z. Functional Nanostructured Surfaces in Hybrid Sol−gel Glass in Large Area for Antireflective and Super-hydrophobic Purposes. *J. Mater. Chem.* **2012**, *22*, 17328−17331.

(7) Tang, P.; Zhang, W.; Wang, Y.; Zhang, B.; Wang, H.; Lin, C.; Zhang, L. Effect of Superhydrophobic Surface of Titanium on Staphylococcus Aureus Adhesion. *J. Nanomater.* **2011**, *2011*, 1−8.

(8) Fadeeva, E.; Truong, V. K.; Stiesch, M.; Chichkov, B. N.; Crawford, R. J.; Wang, J.; Ivanova, E. P. Bacterial Retention on Superhydrophobic Titanium Surfaces Fabricated by Femtosecond Laser Ablation. *Langmuir* **2011**, *27*, 3012−3019.

(9) Ivanova, E. P.; Hasan, J.; Webb, H. K.; Truong, V. K.; Watson, G. S.; Watson, J. A.; Baulin, V. A.; Pogodin, S.; Wang, J. Y.; Tobin, M. J.; Lobbe, C.; Crawford, R. J. Natural Bactericidal Surfaces: Mechanical Rupture of Pseudomonas Aeruginosa Cells by Cicada Wings. *Small* **2012**, *8*, 2489−2494.

(10) Pogodin, S.; Hasan, J.; Baulin, V. A.; Webb, H. K.; Truong, V. K.; Phong Nguyen, T. H.; Boshkovikj, V.; Fluke, C. J.; Watson, G. S.; Watson, J. A.; Crawford, R. J.; Ivanova, E. P. Biophysical Model of Bacterial Cell Interactions with Nanopatterned Cicada Wing Surfaces. *Biophys. J.* **2013**, *104*, 835−840.

(11) Yao, C.; Webster, T. J.; Hedrick, M. Decreased Bacteria Density on Nanostructured Polyurethane. *J. Biomed. Mater. Res., Part A* **2014**, *102*, 1823−1828.

(12) Hench, J. J.; Strakos, Z. The RCWA Method - a Case Study with Open Questions. *Electron. Trans. Numer. Anal.* **2008**, *31*, 331−357.

(13) O'Neill, F.; Gower, M. C.; Turcu, I. C.; Owadano, Y. X-ray Lithography Using a KrF Laser-plasma Source. *Appl. Opt.* **1986**, *25*, 464−465.

(14) Kang, H. J.; Cho, S. U.; Kim, E. S.; Kim, C.-S.; Jeong, M. Y. Improving Light-emitting Diode Performance through Sapphire Substrate Double-side Patterning. *Opt. Eng.* **2013**, *52*, 023002−023002.

(15) Kurihara, M.; Hatakeyama, S.; Yamada, N.; Shimomura, T.; Nagai, T.; Yoshida, K.; Tomita, T.; Hoga, M.; Hayashi, N.; Ohtani, H.; Fujihira, M. Characterization of Antisticking Layers for UV Nanoimprint Lithography Molds with Scanning Probe Microscopy. *Jpn. J. Appl. Phys.* **2010**, *49*, 06GL02.

(16) Kim, S. H.; Park, G.; Hyun, H.; Lee, J. H.; Ashitate, Y.; Choi, J.; Hong, G. H.; Owens, E. A.; Henary, M.; Choi, H. S. Near-infrared Lipophilic Fluorophores for Tracing Tissue Growth. *Biomed. Mater.* **2013**, *8*, 014110.

(17) Lee, J. H.; Park, S.; Hyun, H.; Bordo, M. W.; Oketokoun, R.; Nasr, K. A.; Frangioni, J. V.; Choi, H. S. High-throughput Screening of Small Molecule Ligands Targeted to Live Bacteria Surface. *Anal. Chem.* **2013**, *85*, 3508−3514.

(18) Kim, S. H.; Lee, J. H.; Hyun, H.; Ashitate, Y.; Park, G.; Robichaud, K.; Lunsford, E.; Lee, S. J.; Khang, G.; Choi, H. S. Near-infrared Fluorescence Imaging for Noninvasive Trafficking of Scaffold Degradation. *Sci. Rep.* **2013**, *3*, 1198.

(19) Tsakadze, Z. L.; Ostrikov, K.; Xu, S. Low-temperature Assembly of Ordered Carbon Nanotip Arrays in Low-frequency, High-density Inductively Coupled Plasmas. *Surf. Coat. Technol.* **2005**, *191*, 49−53.

(20) Cheng, Y. T.; Rodak, D. E.; Wong, C. A.; Hayden, C. A. Effects of Micro- and Nano-Structures on the Self-cleaning Behaviour of Lotus Leaves. *Nanotechnology* **2006**, *17*, 1359−1362.

(21) Gardel, M.; Schwarz, U. Cell-substrate Interactions. *J. Phys.: Condens. Matter* **2010**, *22*, 190301.

(22) van Loosdrecht, M. C.; Lyklema, J.; Norde, W.; Zehnder, A. J. Influence of Interfaces on Microbial Activity. *Microbiol. Rev.* **1990**, *54*, 75−87.

(23) Harkes, G.; Feijen, J.; Dankert, J. Adhesion of Escherichia Coli on to a Series of Poly(methacrylates) Differing in Charge and Hydrophobicity. *Biomaterials* **1991**, *12*, 853−860.

(24) An, Y. H.; Friedman, R. J. Concise Review of Mechanisms of Bacterial Adhesion to Biomaterial Surfaces. *J. Biomed. Mater. Res.* **1998**, *43*, 338−348.

(25) Marmur, A. The Lotus Effect: Superhydrophobicity and Metastability. *Langmuir* **2004**, *20*, 3517−3519.

(26) Marshall, K. C. Mechanisms of Bacterial Adhesion at Solid-water Interfaces. In *Bacterial Adhesion;* Savage, D. C.; Fletcher, M., Eds.; Springer: New York, 1985; Chapter 6, pp 133−161.

(27) Vacheethasanee, K.; Marchant, R. Nonspecific Staphylococcus Epidermidis Adhesion. In *Handbook of Bacterial Adhesion;* An, Y. H.; Friedman, R., Eds.; Humana Press: New York, 2000; Chapter 5, pp 73−90.



DOI: 10.1021/am506254r
*ACS Appl. Mater. Interfaces* 2015, 7, 326−331